Disorder-assisted distribution of entanglement in XY spin chains

Guilherme M. A. Almeida,[1,*] Francisco A. B. F. de Moura,[1] Tony J. G. Apollaro,[2,3] and Marcelo L. Lyra[1]

[1]*Instituto de Física, Universidade Federal de Alagoas, 57072-900 Maceió, Alagoas, Brazil*

[2]*Quantum Technology Lab, Dipartimento di Fisica, Università degli Studi di Milano, 20133 Milano, Italy*

[3]*Centre for Theoretical Atomic, Molecular, and Optical Physics, School of Mathematics and Physics, Queen's University Belfast, Belfast BT7 1NN, United Kingdom*

(Received 18 July 2017; published 11 September 2017)

We study the creation and distribution of entanglement in disordered XY-type spin-1/2 chains for the paradigmatic case of a single flipped spin prepared on a fully polarized background. The local magnetic field is set to follow a disordered long-range-correlated sequence with power-law spectrum. Depending on the degree of correlations of the disorder, a set of extended modes emerges in the middle of the band yielding an interplay between localization and delocalization. As a consequence, a rich variety of entanglement distribution patterns arises, which we evaluate here through the concurrence between two spins. We show that, even in the presence of disorder, the entanglement wave can be pushed to spread out, reaching distant sites, and also to enhance pairwise entanglement between the initial site and the rest of the chain. We also study the propagation of an initial maximally entangled state through the chain and show that correlated disorder improves the transmission quite significantly when compared with the uncorrelated counterpart. Our work contributes in designing solid-state devices for quantum information processing in the realistic setting of correlated static disorder.

DOI: 10.1103/PhysRevA.96.032315

I. INTRODUCTION

In the past few decades, since the seminal proposal put forward by Bose [1], much attention has been given to solid-state hardware where information is encoded in stationary spins acting as *qubits* in which the energy splitting is induced by a local magnetic field and the (usually nearest-neighbor) coupling between them is set by their exchange interaction. Following that, it has been shown that low-dimensional spin chains can act as efficient (especially for short-distance communication) quantum "wires" for carrying out quantum-state transfer protocols [1–11] as well as creation and distribution of entanglement [12–21], both being pivotal tasks in quantum networks [22]. Physically, spin chains may be implemented in many platforms such as NMR systems [23], optical lattices [24,25], arrays of coupled cavity-QED systems [26,27], superconducting circuits [28], nitrogen vacancies in diamond [29], and waveguides [30].

The main advantages of using spin chains as quantum channels are twofold. First, they bypass the need for interconverting between photons and qubits, such as in hybrid light-matter devices [22,27,31], which demands a high degree of control and may lead to decoherence and losses. Moreover, most of the protocols require minimal user control (mostly at the sender and receiver sites) as the system's dynamics is driven through the evolution of the underlying Hamiltonian, offering thus a versatile toolbox for quantum information processing purposes. The analytic tractability of the spin Hamiltonian has allowed for several theoretical investigations. For instance, a specific modulation of the entire chain allows for perfect state transfer as shown in Refs. [2,3] (see also Ref. [32]). By adding in local defects, either in the form of magnetic fields or coupling strengths, it is possible to carry out high-fidelity quantum-state transfer (it takes place by effectively reducing the operating Hilbert space) [4,6,7,10,11,33] and routing protocols [34–36], and to control and enhance entanglement distribution [13,14]. Also, it has been shown that gapped dimerized models play a major role in establishing long-distance communication [6,17,19,21,27,33].

All these essential tasks that can be performed using spin chains rely on how precisely its parameters can be tuned. Thereby, the very task of engineering those systems poses a few challenging issues. First of all, it is not trivial to address a single spin with the desired precision although significant progress has been achieved [24]. Another crucial one is due to fabrication errors (e.g., spin positioning) which lead to disorder and thus localization of quantum information [37,38]. Since experimental imperfections may always be present in solid-state devices, it becomes essential to analyze their robustness to that and check whether it is even possible to enhance transfer of information through noisy channels [16,37,39–46]. Most of the works in this direction have addressed the effects of site-independent random fluctuations (static disorder), and the general verdict is that some protocols are prone to survive it as long as disorder does not overcome a given threshold.

It is well established that single-particle eigenstates of one-dimensional (1D) tight-binding models featuring random potentials are all exponentially localized no matter how strong the disorder is [47]. This is, however, no longer true when internal correlations in the disorder distribution are present. It was shown that short-range spatial correlations induce the breakdown of Anderson localization, thereby elucidating transport properties for a wide class of polymers [48]. Following the road, it was demonstrated that long-range correlations [49,50] promote the appearance of a band of extended states with well-defined mobility edges separating them from localized states, thus revealing an Anderson-like metal-insulator transition. That was later confirmed using single-mode waveguides [51], and many related experiments have been carried out since then [52] (see Ref. [53] for a recent review on the subject). Right after the above findings

*gmaalmeida.phys@gmail.com

took place, there has been tremendous interest in investigating dynamical properties of various 1D models featuring either diagonal (on-site potential) or off-diagonal (hopping strength) correlated disorder [54–57]. In particular, it was shown that the one-magnon spectrum of ferromagnetic chains [54] can exhibit a phase of low-energy delocalized states, thus displaying a rich set of dynamical regimes.

Generally speaking, the interplay between localized and delocalized states sets a suitable ground for designing quantum information processing protocols and that is exactly where our work fits in. Here we address how long-range-correlated diagonal disorder affects the transport of quantum information in spin chains. Specifically, we aim to track down the entanglement wave produced after a tiny disturbance on the fully polarized state, that is, a single flipped spin set in the bulk of an isotropic XY chain. This is a rather paradigmatic scenario and has been tackled in recent experiments [25].

In this work, the local magnetic field is set to follow a disorder distribution with power-law spectrum of the form $S(k) \propto 1/k^{\alpha}$, where k is the corresponding wave number and α accounts for the degree of long-range correlations. We emphasize that such a kind of long-range-correlated disorder must not be viewed solely as an imposed scenario on the spin chain. In fact, many stochastic processes in nature featuring long-range correlations are expected to obey a power-law spectrum, such as, to name a few examples, nucleotide sequences in DNA molecules [58], which may strongly affect electronic transport, plasma fluctuations [59], and patterns in surface growth [60]. Therefore, on the one hand, fluctuations arising from the fabrication of solid-state quantum information devices might not always be completely random, i.e., uncorrelated. On the other hand, instead of trying to impose a set of finely tuned parameters, it should be more realistic, on the experimental side, to devise a scheme that allows for the presence of correlated disorder.

Here, we show that the *degree* of long-range-correlated disorder, α, ultimately controls the entanglement distribution profile after the excitation is released from the middle of the chain following the system's Hamiltonian dynamics. Moreover, we report an enhancement of entanglement between the initial site and the rest of the chain as α goes from zero (uncorrelated disorder) to $\alpha = 2$. For $\alpha > 2$, entanglement becomes more prominent between symmetrically located spins, with respect to the initial site, and their nearest neighbors. Furthermore, we study the propagation of a Bell-type state through the chain and show that the entanglement transmission coefficient (through a given fixed site of the chain) significantly increases with α to the point of surpassing the reflection coefficient.

The remainder of this paper is organized as follows. In Sec. II, we introduce the spin Hamiltonian featuring on-site long-range-correlated disorder. In Sec. III, we briefly discuss the entanglement measurements that are used through the paper. In Sec. IV we discuss the dynamics of entanglement for the ordered chain and show our results for the disordered scenario. Final comments are addressed in Sec. V.

II. SPIN-CHAIN HAMILTONIAN

We consider a one-dimensional isotropic spin chain featuring XX-type exchange interactions as given by the

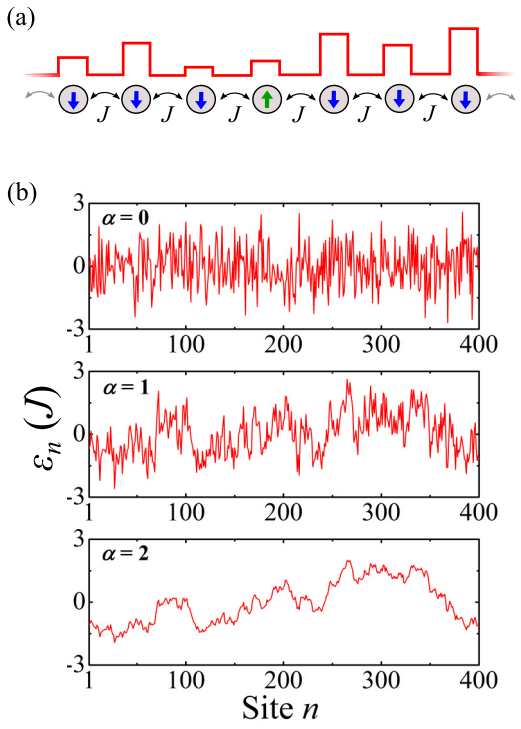

FIG. 1. (a) Sketch of the spin chain featuring XX-type exchange interactions with strength J subjected to a random on-site potential landscape (depicted by red bars). The spin chain is initialized in a fully polarized state and a single excitation (a flipped spin) is set, say, in the middle of it. We thus let it evolve via its Hamiltonian dynamics. (b) Single realization of the disorder distribution $\{\varepsilon_n\}$ (in units of J) generated from Eq. (3) for $\alpha = 0$, 1, and 2, and $N = 400$. The entire sequence is normalized satisfying $\langle \epsilon_n \rangle = 0$ and $\langle \epsilon_n^2 \rangle = 1$. We note that by increasing α the distribution smooths out, resembling the trace of a fractional Brownian motion (see the last panel for $\alpha = 2$).

Hamiltonian ($\hbar = 1$)

$$\hat{H}_S = \sum_{n=1}^{N} \frac{\varepsilon_n}{2}\left(\hat{1} - \hat{\sigma}_n^z\right) - \sum_{n=1}^{N-1} \frac{J_n}{2}\left(\hat{\sigma}_n^x \hat{\sigma}_{n+1}^x + \hat{\sigma}_n^y \hat{\sigma}_{n+1}^y\right), \quad (1)$$

where $\hat{\sigma}_n^{x,y,z}$ are the usual Pauli operators for the nth spin, ε_n is the strength of the local magnetic field, and J_n is the exchange coupling rate. The above Hamiltonian can be put into another equivalent form through the Jordan-Wigner transformation which maps the spin Hamiltonian (1) onto a system of noninteracting spinless fermions,

$$\hat{H} = \sum_{n=1}^{N} \varepsilon_n \hat{c}_n^{\dagger}\hat{c}_n - \sum_{n=1}^{N-1} J_n(\hat{c}_n^{\dagger}\hat{c}_{n+1} + \hat{c}_{n+1}^{\dagger}\hat{c}_n), \quad (2)$$

where $\hat{c}_n^{\dagger}$ ($\hat{c}_n$) creates (annihilates) a particle at the nth site. That way, the presence (absence) of a fermion in a given site represents a spin-up (spin-down) state. Note that since $[\hat{H}, \sum_n \hat{c}_n^{\dagger}\hat{c}_n] = 0$, Hamiltonian (2) can be split into number-invariant subspaces. Here, we aim to study the entanglement generated from a single particle prepared in a given location on top of the fully polarized state $|\text{vac}\rangle \equiv |00\cdots0\rangle$ [see Fig. 1(a)]. Thereby, the whole dynamics takes place in the

single-excitation sector $\{|n\rangle\}$, with $|n\rangle \equiv \hat{c}_n^\dagger|\text{vac}\rangle$, and Eq. (2) takes the form of an $N\times N$ tridiagonal hopping matrix.

Now, let us make a few considerations about the parameters of the chain. First, we set a uniform distribution of hopping rates (exchange interaction) $J_n = J$. The on-site potentials (local magnetic fields), however, will follow a disorder distribution of a special kind. Disorder can arise from manufacturing imperfections and/or due to dynamical factors. Either way, we can safely assume that the noise is static; that is, it does not change considerably over time. Here we consider random sequences featuring long-range spatial correlations, and one of the most simple and convenient ways to model it is by considering the trace of a fractional Brownian motion with power-law spectrum $S(k) \propto 1/k^\alpha$ which can be built from [49,56]

$$\varepsilon_n = \sum_{k=1}^{N/2} k^{-\alpha/2}\cos\left(\frac{2\pi nk}{N} + \phi_k\right), \tag{3}$$

where $k = 1/\lambda$ and λ is the wavelength of the modulation profile, $\{\phi_k\}$ are random phases uniformly distributed within $[0,2\pi]$, and α ultimately accounts for the degree of correlations. Hereafter, we normalize the above sequence to have zero mean and unit variance, which can be done by simply redefining $\varepsilon_n \to (\varepsilon_n - \langle\varepsilon_n\rangle)/\sqrt{\langle\varepsilon_n^2\rangle - \langle\varepsilon_n\rangle^2}$. We emphasize that the disorder distribution generated by the above formalism has no typical length scale, which is a characteristic of several stochastically generated natural series [61]. The power-law spectral density $S(k) \propto 1/k^\alpha$ is a direct consequence of the power-law form of the two-point correlation function. Indeed, α is related to the Hurst exponent [62] through $H = (\alpha - 1)/2$. This quantity describes the self-similarities of the series and also the persistence of its increments. For $\alpha = 0$, the sequence is completely uncorrelated, whereas for any value $\alpha > 0$ intrinsic long-range correlations appear. The value $\alpha = 2$ represents the case in which the sequence mimics the trace of a Brownian motion. When $\alpha > 2$ ($\alpha < 2$) the increments on the series are said to be persistent (antipersistent).

In Fig. 1(b) we show samples generated by Eq. (3) for different values of α. For $\alpha = 0$ we recover the standard uncorrelated disorder (white noise) distribution where $\langle\varepsilon_i\varepsilon_j\rangle = \langle\varepsilon_i^2\rangle\delta_{i,j}$. For $\alpha > 0$, internal correlations take place, giving rise to the trace of a Brownian motion when $\alpha = 2$. The sequence becomes less rough as we further increase the parameter α [49]. Interestingly, it was shown in Ref. [49] for a tight-binding electronic model that the fractal nature of the potential landscape arising from Eq. (3) dictates the appearance of delocalized electronic states around the band center of the one-particle spectrum when $\alpha > 2$. Those are kept apart from localized states by two mobility edges. Similar behavior was also reported in Refs. [50,54,55].

Here we investigate how the interplay between localized and delocalized modes affects the dynamics of entanglement in XY spin chains described by Hamiltonian (2), which has the form of a standard hopping model. Right before that, let us first illustrate the tools we adopt to quantify entanglement.

III. QUANTIFYING ENTANGLEMENT

Here we deal with two common measures of bipartite entanglement, namely, the von Neumann entropy, which addresses the amount of entanglement a given subsystem (say, a spin block) is sharing with the rest the chain (the whole system being in a pure state), and the so-called concurrence [63], which is the most suitable tool for characterizing entanglement between two qubits in an arbitrary mixed state.

Let us consider a *single* quantum particle hopping on a network with N sites modeled by a Hamiltonian of the form of Eq. (2). Note that this hopping particle may represent an *actual* fermion or boson, or, which is our case, a single flipped spin propagating along the chain via exchange interactions [cf. Eqs. (1) and (2)]. Generally speaking, whenever we mention *qubit*, we mean the two logical states $|0_i\rangle$ and $|1_i\rangle$ corresponding to the eigenstates of $\hat{\sigma}_i^z$. Furthermore, because of the conservation of the total magnetization in the z direction and the presence of at most one flipped spin in the chain, $|0_i\rangle$ ($|1_i\rangle$) matches with the absence (presence) of a fermion at the ith site.

Any given arbitrary state in the single-particle sector can be written as a linear combination of the single-excitation basis $\{|i\rangle\}$, that is,

$$|\psi\rangle = \sum_i w_i|i\rangle, \tag{4}$$

with w_i being a complex coefficient in such a way that $|w_i|^2$ is the probability of finding the particle at site i. In the density operator formalism, it reads

$$\rho = |\psi\rangle\langle\psi| = \sum_i\sum_j w_i w_j^*|i\rangle\langle j|. \tag{5}$$

Now suppose we want to write down the state for a block of spins $\mathcal{A}_L$ of size L. This can be done by choosing a specific set of sites and *tracing out* the rest of them, $\rho_L = \text{Tr}_{\mathcal{B}_{N-L}}\rho$, where $\mathcal{B}_{N-L}$ denotes the remaining set. The resulting reduced density operator, expressed in its diagonal basis, is given by $\rho_L = \text{diag}[p, 1-p]$, where $p \equiv \sum_{i\in\mathcal{A}_L}|w_i|^2$. A quite straightforward way to compute the entanglement between both partitions $\mathcal{A}$ and $\mathcal{B}$, given that the overall state is pure, is through the well-known von Neumann entropy

$$S[\rho_L] = -\text{Tr}\rho_L\log_2\rho_L = -p\log_2 p - (1-p)\log_2(1-p), \tag{6}$$

which in our case is bounded by the interval $[0,1]$, with 0 accounting for a product (separable) state and 1 for a fully entangled one. The entropy above thus depends only on the total probability p of finding the excitation within block $\mathcal{A}_L$, reaching its maximum when $p = 1/2$.

In order to characterize how much entanglement can be found in a given pair of spins, say i and j, we once again evaluate the reduced density operator which, in the basis $\{|0_i0_j\rangle, |1_i0_j\rangle, |0_i1_j\rangle, |1_i1_j\rangle\}$, reads

$$\rho_{i,j} = \begin{bmatrix} 1-|w_i|^2-|w_j|^2 & 0 & 0 & 0 \\ 0 & |w_i|^2 & w_i w_j^* & 0 \\ 0 & w_j w_i^* & |w_j|^2 & 0 \\ 0 & 0 & 0 & 0 \end{bmatrix}. \tag{7}$$

The two-site reduced density matrix above is all we need to evaluate the amount of entanglement shared by the pair of spins through the concurrence [63] which, given a general bipartite

mixed state ρ_{AB} of two qubits, is defined by

$$C(\rho_{AB}) = \max\{0, \sqrt{\lambda_1} - \sqrt{\lambda_2} - \sqrt{\lambda_3} - \sqrt{\lambda_4}\}, \quad (8)$$

where $\{\lambda_i\}$ are the eigenvalues, in decreasing order of the non-Hermitian matrix $\rho_{AB}\tilde{\rho}_{AB}$, where

$$\tilde{\rho}_{AB} = (\hat{\sigma}_y \otimes \hat{\sigma}_y)\rho^*_{AB}(\hat{\sigma}_y \otimes \hat{\sigma}_y) \quad (9)$$

and ρ^*_{AB} is the complex conjugate of ρ_{AB}. For separable qubits, we have $C = 0$. On the other hand, for fully entangled particles, $C = 1$. In our case, Eq. (7), the concurrence reads

$$C_{i,j} \equiv C(\rho_{i,j}) = 2|w_i w_j|; \quad (10)$$

that is, it depends only on the wave-function amplitude of both spins of interest.

IV. TIME EVOLUTION OF ENTANGLEMENT

In this section, we investigate the time evolution of entanglement in the spin chain described by Hamiltonian (1) in the presence of random on-site potentials (local magnetic fields) featuring long-range spatial correlations [see Eq. (3)] starting from a fully localized spin excitation in the bulk of a polarized background.

A. Pure chain

We start off our discussion for the noiseless case, that is, $\varepsilon_i = \varepsilon$. The dynamics of entanglement for the uniform chain has already been studied in a very detailed way in Ref. [12]. For completeness, we now briefly recall the main aspects of it. That settles the grounds for our following investigation.

Given the unitary evolution, $|\psi(t)\rangle = \hat{\mathcal{U}}(t)|\psi(0)\rangle$, where $\hat{\mathcal{U}}(t) \equiv e^{-i\hat{H}t}$ is the unitary time-evolution operator, we have, in terms of the spectral decomposition of the Hamiltonian,

$$|\psi(t)\rangle = e^{-iHt}|\psi(0)\rangle = \sum_k e^{-iE_k t}|E_k\rangle\langle E_k|\psi(0)\rangle. \quad (11)$$

For a translational-invariant array, the normal modes are well known (plane waves) and read

$$E_k = 2J\cos(k/2), \quad (12)$$

$$|E_k\rangle = \sqrt{\frac{2}{N+1}}\sum_{x=1}^{N}\sin\frac{kx}{2}|x\rangle, \quad (13)$$

with $k = 2\pi m/(N+1)$ and $m = 1, \ldots, N$. Given a fully localized initial state at site x_0, $|\psi(0)\rangle = |x_0\rangle$, the evolved state features coefficients (herein we take $J = 1$ or, equivalently, $t \to tJ$)

$$w_x(t) = \langle x|\psi(t)\rangle = \frac{2}{N+1}\sum_k e^{i2\cos(k/2)t}\sin(kx)\sin(kx_0), \quad (14)$$

where the probability of finding the spin excitation at position x is simply the absolute square of the above expression, $|\langle x|\psi(t)\rangle|^2$.

In this work, despite considering the spin chain to be essentially finite, we are interested in studying the entanglement distribution in the neighborhood of the initial site *before* the excitation reaches the boundaries. Thereby, we can effectively work in the thermodynamic limit $N \to \infty$ where Eq. (14) takes the convenient form [12,64,65]

$$w_x(t) = i^{|x-x_0|}J_{|x-x_0|}(2t), \quad (15)$$

where $J_\nu(z)$ is the νth Bessel function of the first kind. From the properties of the Bessel functions, its maximum amplitude decays as $1/\sqrt{m}$, where $m \equiv |x - x_0|$ is the distance from the initial flipped spin. This maximum is associated with the *first* root of the derivative of the Bessel function, which we denote by z^*_m. Using $d[z^m J_m(z)]/dz = z^m J_{m-1}(z)$, one can easily show that

$$z^*_m = m\frac{J_m(z^*_m)}{J_{m-1}(z^*_m)} \quad (16)$$

(note that $dJ_m(z)/dz = 0$ at $z = z^*_m$). Straightforward numerical analysis shows that $z^*_m \approx m$ for the first root. Therefore, the wave function reaches a given site roughly at $t \approx m/2$ and, after reaching its first maximum, it goes on oscillating with the same frequency but decaying as $1/\sqrt{t}$.

Keeping in mind what has been discussed above, one may grasp the concurrence behavior right away [see Eqs. (10) and (15)]. Basically, the excitation spreads out ballistically from the origin in the form of two dispersing envelopes as shown in Fig. 2(a). Entanglement turns out to be concentrated at the front wave packet corresponding to the first local maximum occurring when $t \approx m/2$, in which the corresponding site becomes *mostly* entangled with its first neighbors as well as with equidistant sites due to the symmetric nature of the wave function [see Fig. 2(b)]. This very region also gets partially entangled with the remaining sites wherever there is a nonvanishing wave amplitude. The concurrence then goes on decaying with time and oscillating with a well-defined period [12].

In summary, in a completely uniform chain the excitation, as well as the entanglement, tends to become homogeneously distributed across the chain, for sufficiently long times, due to the extended nature of the underlying eigenstates [see Eq. (13)] regardless of the initial conditions. Take, for instance, an initial entangled Bell state of the form $(|0_i 1_j\rangle \pm |1_i 0_j\rangle) \otimes |\text{vac}\rangle/\sqrt{2} = (|i\rangle \pm |j\rangle)/\sqrt{2}$. In this case, the wave-function coefficients [Eq. (15)] can be expressed as [12]

$$w_\ell(t) = \frac{1}{\sqrt{2}}[J_{\ell-i}(2t) + i^{(i-j)}J_{\ell-j}(2t)]. \quad (17)$$

There are no qualitative differences between initializing the system with a single excitation or a maximally entangled Bell state of the above form—the latter case will feature different interference profiles in between both initial sites depending on the distance between them—as both access the same set of eigenstates during the evolution. Because of that, here we focus on the case of a single flipped spin prepared on a polarized background. Moreover, this problem has been addressed experimentally [25] using ultracold atoms in optical lattices to study entanglement propagation.

The dynamics discussed above can be seen as a protocol for generating entanglement between distant sites through the natural evolution of the spin chain [1,3,4,8,34], though it gradually becomes weaker with distance due to dispersive effects

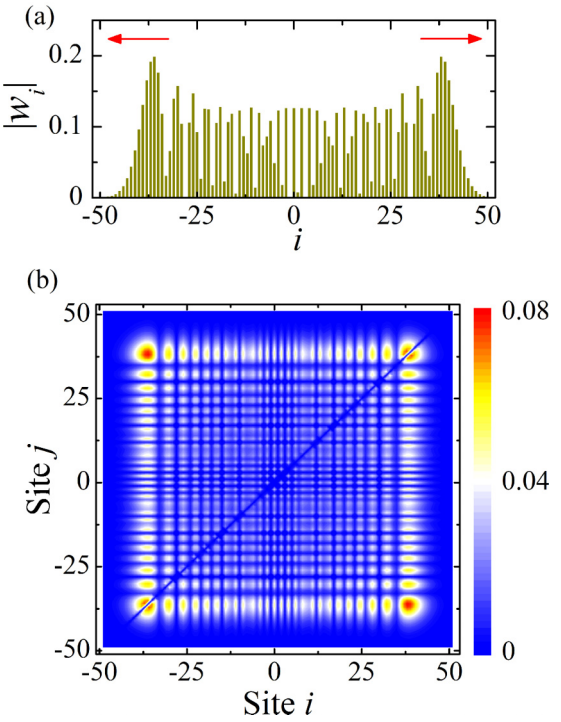

FIG. 2. (a) Wave-function amplitude distribution for the ordered case when $tJ = 20$ for an excitation initially prepared at site 0. It propagates outwards reaching distant sites at $t \approx m$, with m being the distance from the origin. (b) Corresponding entanglement distribution profile measured by the concurrence $C_{i,j}$. Note that the "entanglement wave" mostly involves pairwise correlations between the sites located within the largest wave amplitude and the rest of the chain. Basically, this checkerboard pattern is maintained while the concurrence evolves and tends to become homogeneously distributed after a long time. Both plots were obtained directly from Eqs. (10) and (15).

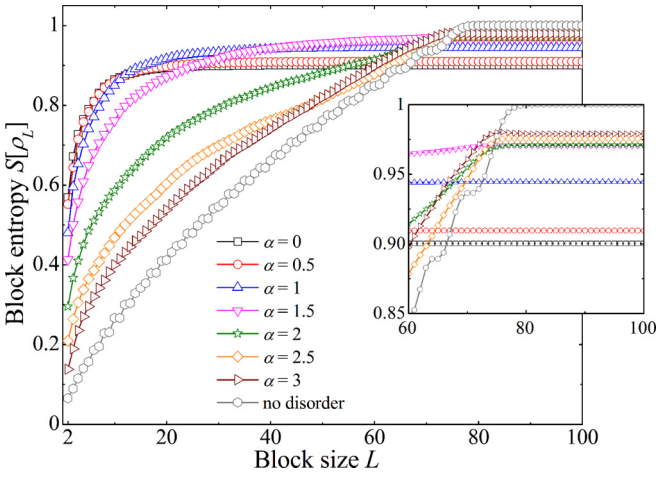

FIG. 3. Entropy for a block of spins, $S[\rho_L]$, versus its size L when $tJ = 40$ for many disorder regimes provided by α including uncorrelated disorder ($\alpha = 0$) and the noiseless condition. Each block involves groups of spins ranging from $(x_0 + 1)$-th to the L-th spin, with x_0 being the initial site (which is out of the block) located in the middle of the chain. The entanglement saturation threshold sets the extension of the wave-function in a given time. Note it happens quite rapidly for lower values of α. The inset provides a zoomed-in view of the saturation region for higher values of α. Plots were obtained from exact numerical diagonalization of Hamiltonian (2) for $N = 400$ and $S[\rho_L]$ was averaged over 10^2 independent realizations of disorder.

(since the chain is uniform). However, this entanglement may be properly distilled into pure singlets [1,66], thus building up resources for quantum teleportation schemes.

B. Disordered chain

By adding uncorrelated on-site disorder to the system, the above scenario changes dramatically. In one-dimensional tight-binding models, the presence of disorder is well known for inducing Anderson localization [47] of every eigenstate no matter how weak the disorder is. Each mode gets exponentially localized around a site, that is, $\langle x|E_k\rangle \sim e^{-\frac{|x-x_0|}{\xi_k}}$ for a given x_0, where ξ_k accounts for the length of localization [67]. As a consequence, the excitation is unable to spread out too far from the origin and so entanglement remains concentrated there for all times [cf. Eq. (10)]. On the other hand, by adding correlations in the disorder distribution, particularly long-ranged correlations, the emergence of extended states in the middle of the band [49,54,56] and their interplay with localized states beyond the mobility edges bring in very interesting resources for entanglement distribution as we are going to show now.

In order to see how far the initial excitation propagates depending on the degree of correlation α [see Eq. (3)], let us first analyze the entanglement entropy for a given block of spins $\mathcal{A}_L$ of size L as defined in Eq. (6). We initialize the system as a single flipped spin located at the middle of the chain (say, the zeroth site $|x_0 = 0\rangle$) and evaluate the block entropy for increasing L where each block begins from the first-neighbor site $x_0 + 1$ and goes forward until the Lth site. The reason for choosing such a partition is the following: As the block entropy, Eq. (6), solely depends on the overall probability of finding the excitation *inside* the block, whenever its saturation occurs for a given value of L, in a given instant, it means that the excitation has not yet reached (or never will reach) the subsequent sites (that is, $x > L$ and $x < -L$). Moreover, the saturation value accounts for how much the initial site is still populated. Note that the wave function spreads out symmetrically and, as already mentioned, the entropy reaches its maximum value, that is, 1, when $p = 1/2$.

The behavior of the entanglement entropy as a function of the block size L is reported in Fig. 3 for several disorder configurations (including the noiseless case for comparison). We stress that every quantity shown in this work is properly averaged over about 10^2 *independent* disorder realizations. In Fig. 3 we note that each curve saturates after crossing a threshold value for L, as mentioned before. This indicates the spot after which $p = \sum_{i\in\mathcal{A}_L} |w_i|^2$ is no longer added up. The saturation takes place quite fast, as expected, for the uncorrelated disorder scenario ($\alpha = 0$) in which pure Anderson localization sets in. A similar profile is maintained for low degrees of correlation, though for higher L. The behavior suddenly changes for $\alpha = 2$ and above, where the disordered potential landscape is characterized by self-similar persistent increments [see Fig. 1(b)]. Now, the entropy slowly increases

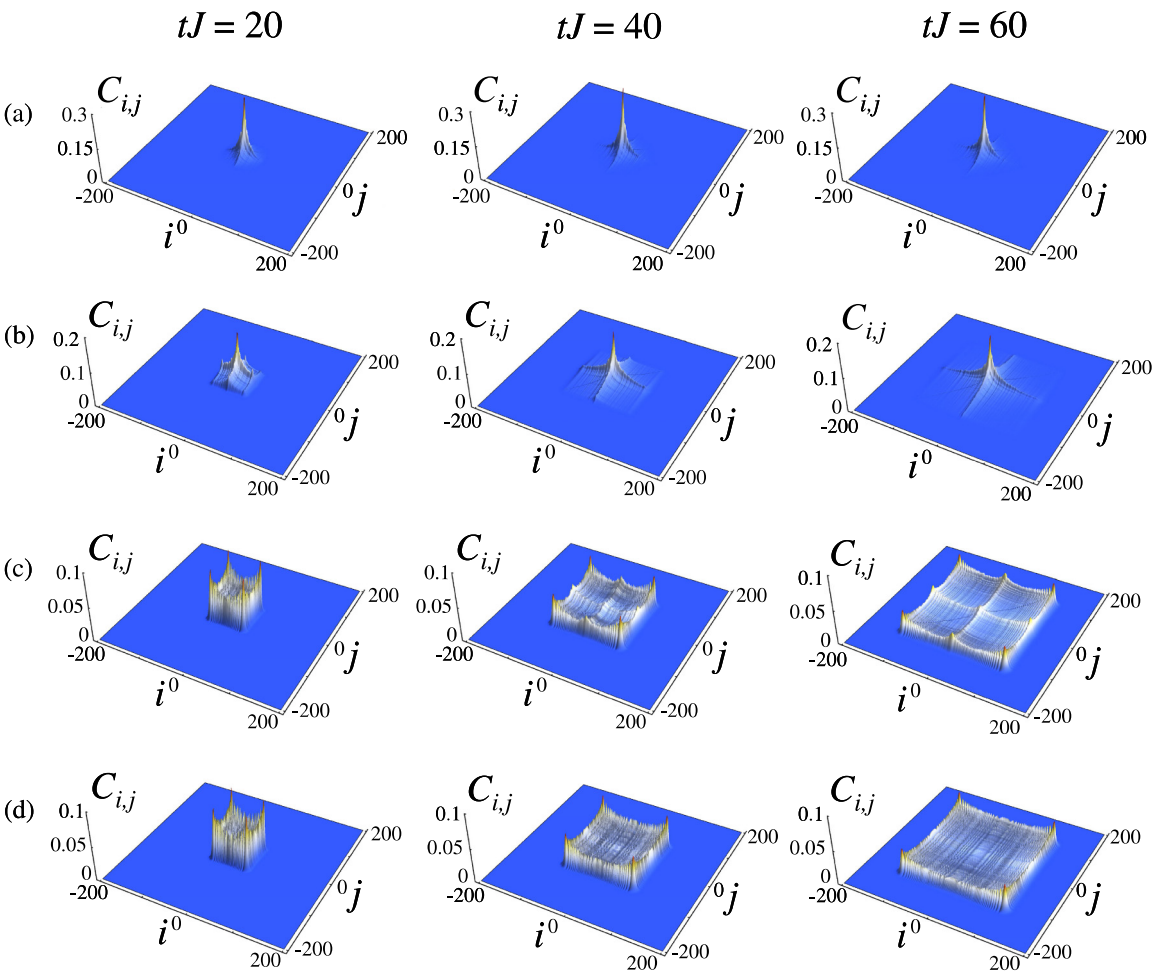

FIG. 4. Snapshots of concurrence distribution for (a) $\alpha = 0$ (uncorrelated disorder), (b) $\alpha = 1$, (c) $\alpha = 2$, and (d) $\alpha = 3$ averaged over 10^2 independent realizations of disorder. The initial state was set in the middle of a chain with $N = 2048$ sites. We set $C_{i,j} = 0$ for $i = j$. The first, second, and third columns correspond to times $tJ = 20$, 40, and 60, respectively. Here, we clearly see that long-range correlations in the disorder distribution push the entanglement wave to reach distant sites, first extending the localization length and then setting up genuine propagating modes when $\alpha = 2$ and higher.

with L indicating that extended states are indeed taking part in the evolution. Therefore, $\alpha = 2$ marks the transition point between the localized and delocalized regimes [49,56]. We discuss how it affects the distribution of entanglement in a moment. Note that the excitation has reached out about the 80th spin corresponding to the ordered curve, which is the farthest it can go for $tJ = 40$ [cf. Eq. (16)]. Also, since in this case the entropy goes to 1, the excitation has almost completely left the initial site (see inset of Fig. 3).

Now, let us take a more detailed view on the way entanglement is distributed between a pair of spins along the chain in the disordered scenario. Figure 4 shows time snapshots of the concurrence grid for several values of α. In the case of uncorrelated disorder [Fig. 4(a)], the concurrence barely propagates, as expected, since the spin excitation remains strongly localized at the initial site. The slightest amount of long-range correlations in the disorder distribution allows for a broader distribution of entanglement. Already for $\alpha = 1$ in Fig. 4(b), the concurrence between the initial site and the remaining ones extends further out. In other words, the localization length effectively increases. Interestingly, a closer look at the first panel of Fig. 4(b) (that is, for $tJ = 20$) indicates the appearance of a (very) small envelope surrounding the central peak that rapidly dissipates with time. This is signaling the emergence of weakly localized modes [49,54,56] although the dynamics is still ruled by the strongly localized modes. As we saw in Fig. 3, $\alpha = 2$ sets the transition to a delocalizedlike behavior. In terms of entanglement dynamics [see Fig. 4(c)], the interplay between localized and delocalized states keeps the central spin able to correlate with distant sites. At the same time the propagating wave front responsible for that also generates entanglement between neighboring spins and their equidistant counterpart. If we increase the degree of noise correlations, i.e., by increasing α, the entanglement involving the initial site is substantially decreased [Fig. 4(d)] and the distribution pattern resembles that of the ordered case shown in Fig. 2(b). Indeed, if α is large enough the summation in Eq. (3) reduces to a single cosine function in the asymptotic limit and thus the local magnetic field acquires a smooth periodic behavior in space, thereby suppressing localization.

In order to show the highest amount of pairwise entanglement one is able to create during the process discussed

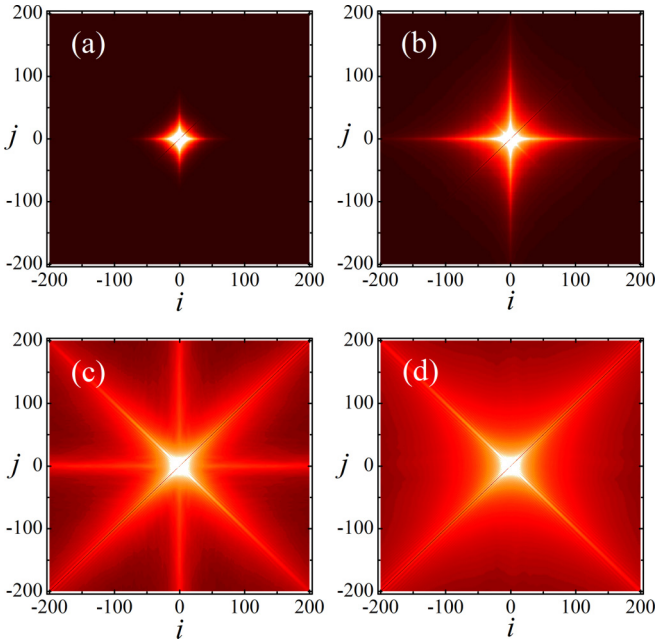

FIG. 5. Maximum concurrence $C_{i,j}^{\max}$ for (a) $\alpha = 0$ (uncorrelated disorder), (b) $\alpha = 1.0$, (c) $\alpha = 2.0$, and (d) $\alpha = 3.0$ averaged over 10^2 independent realizations of disorder. The scale goes from 0 (dark spots) to 0.1 and above (bright spots). The system's parameters are the same as from Fig. 4 and the time window considered for $C_{i,j}^{\max}$ was $tJ \in [0,200]$, thus making sure that the entanglement wave has passed through the neighborhood of the initial site (which we denote as the zeroth site for ease of use) without reaching the boundaries of the chain ($N = 2048$). As we move from uncorrelated disorder towards long-range-correlated disorder, there are many configurations available for entanglement distribution.

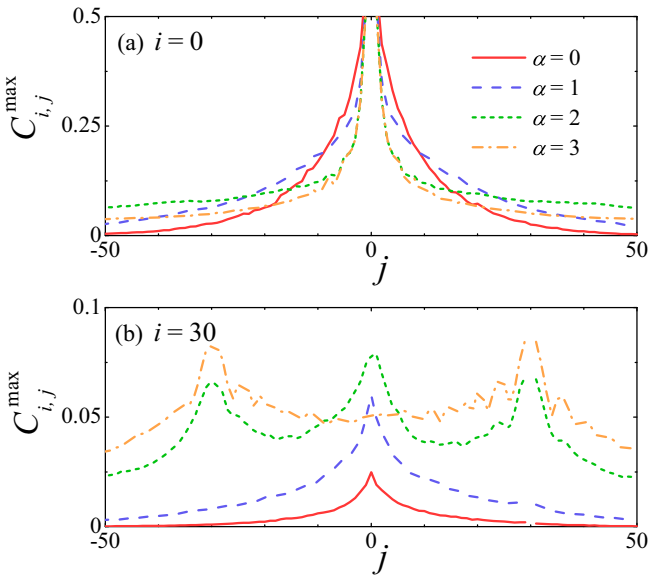

FIG. 6. Distribution of maximum concurrence $C_{i,j}^{\max}$ for fixed (a) $i = 0$ (initial site) and (b) $i = 30$ and varying α. Those are basically detailed side views of Fig. 5 involving a much smaller region. Again, the time window was set to $tJ \in [0,200]$ and $C_{i,j}^{\max}$ was averaged over 10^2 independent realizations of disorder.

above, in Fig. 5 we plot the *maximum* concurrence evaluated in a given time interval. That ultimately provides a bird's-eye view on the way entanglement is shared among individual spins. In Fig. 5(a) the prominent core witnesses the fully localized nature of the underlying Hamiltonian spectrum. For $\alpha = 1$ [Fig. 5(b)], although long-range correlations are already building up, the latter are not enough for breaking down the localized behavior, though the concurrence involving the central site widens out considerably. The value $\alpha = 2$ corresponds to the critical correlation degree signaling the emergence of extended states [49]. In this case, entanglement results from the coexistence between order and disorder, thus inducing propagating modes in the dynamics while keeping some residual localizedlike behavior. This results in the very interesting pattern shown in Fig. 5(c). Extended states then take over the dynamics for higher degrees of correlation as shown Fig. 5(d) for $\alpha = 3$.

Figure 6 provides a more detailed side view of the distribution of $C_{0,j}^{\max}$ [Fig. 6(a)] and $C_{30,j}^{\max}$ [Fig. 6(b)] ranging over about a hundred sites. Note that the central site is able to establish a higher entanglement with distant sites when $\alpha = 2$, suddenly decreasing when $\alpha = 3$. Also, for $\alpha = 2$ and above, note the formation of symmetric peaks accounting for the entanglement in between small groups of neighboring spins and their equidistant parts.

C. Entanglement transmission

So far we have been discussing the generation and spreading of entanglement from the origin and analyzing mostly its distribution patterns as a function of the degree of correlations in the disorder distribution. We now turn our attention to a slightly different problem, which is the task of transmitting entanglement along the chain [1]. Suppose we prepare a maximally entangled state of the form $|\psi(0)\rangle = \frac{1}{2}(|0_s 1_{s'}\rangle + |1_s 0_{s'}\rangle)$ involving spin s, belonging to the chain, and an external (uncoupled) one s'. Because of the Hamiltonian dynamics, the component of the wave function featuring the excitation inside the chain evolves and causes the entanglement, initially present only between site s and s', to get shared among the latter and other spins of the chain. Hence, the figure of merit of the entanglement between a given spin r (belonging to the chain) and the external spin s' is given by $C_r(t) \equiv \sqrt{2}|w_r(t)| = |\langle r|\hat{\mathcal{U}}(t)|s\rangle|$. This can be worked out by using the same dynamics discussed previously.

It should be noted that single-particle states saturate the Coffman-Kundu-Wootters conjecture [68] (see also Ref. [12]), which means that all the entanglement present in the system is encoded by pairwise correlations only (there is no higher-order entanglement). As a consequence, it is easy to check that $\sum_r C_r^2 = 1$. Hence, we can use this fact to build up proper entanglement transmission and reflection coefficients of the form [13]

$$T = \lim_{t\to\infty} \sum_{r>r_0} C_r^2(t), \qquad R = \lim_{t\to\infty} \sum_{r<r_0} C_r^2(t), \tag{18}$$

where r_0 denotes a particular reference spin which the above coefficients stand for.

Figure 7 shows the transmission and reflection coefficients as a function of the degree of correlations α for several

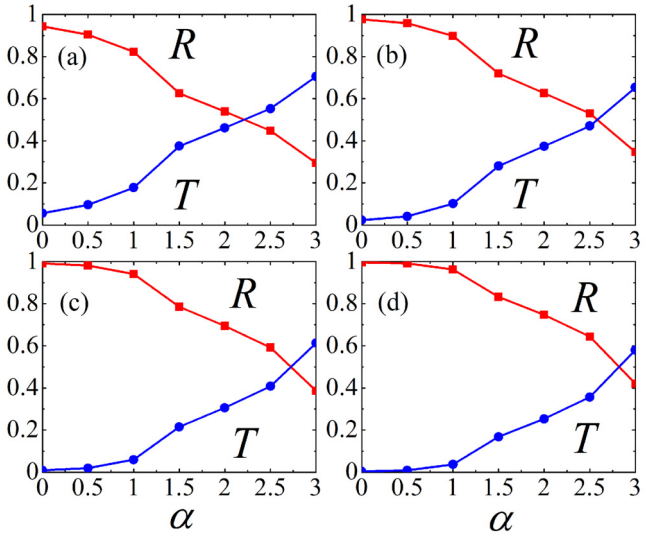

FIG. 7. Entanglement transmission and reflection coefficients [Eq. (18)] versus α for (a) $r_0 = 20$, (b) $r_0 = 30$, (c) $r_0 = 40$, and (d) $r_0 = 50$. The initial state was a maximally entangled pair $|\psi(0)\rangle = \frac{1}{2}(|0_s 1_{s'}\rangle + |1_s 0_{s'}\rangle)$ with the sender prepared in the first site ($s = 1$) in a chain of size $N = 400$ (note that now, for convenience, we are numbering each spin regularly from 1 to N). The calculations were performed without letting the wave function reach the other end of the chain and the coefficients were evaluated at times when $C_r^2(t)$ (averaged over 10^2 samples) achieved a stationary behavior in order to account for the long-time regime.

reference spins r_0. The initial state was $|\psi(0)\rangle = \frac{1}{2}(|s\rangle + |s'\rangle)$, with s denoting the first site in a chain of 400 spins. We stress that all the calculations were performed before the wave function reached the other boundary and T and R were evaluated at times when $C_r^2(t)$ (averaged over the number of realizations) achieved a stationary behavior. Unlike the $\alpha = 0$ (uncorrelated disorder) case, where the transmission coefficient is, for all practical purposes, negligible already when considering the propagation of entanglement across the 20th site of the chain [Fig. 7(a)], there is a quite significant transmission gain when $\alpha \neq 0$. In Fig. 7(a), for instance, it goes from $T \approx 0.05$ to $T \approx 0.7$ when $\alpha = 3$. Even though T slowly diminishes (see Fig. 7) as we get more distant from s, i.e., by increasing r_0 in Eq. (18), we nevertheless see a monotonic increase of the transmission coefficient by increasing the disorder correlations. Furthermore, we note that T surpasses R when $\alpha > 2$, thus once again revealing the presence of delocalized states in the spectrum [49,56].

V. CONCLUDING REMARKS

In our work, we addressed the problem of creating and distributing entanglement in disordered 1D spin chains by means of the time evolution of a single flipped spin prepared on the fully polarized state. We considered on-site diagonal disorder (that is, on the local magnetic field distribution) with long-range spatial correlations resulting from the power-law nature of the spectral density, $S(k) \propto 1/k^{\alpha}$. A rich variety of dynamical regimes for the entanglement we reported here has been generated by varying a single parameter, namely, the degree of correlations in the on-site magnetic field disorder distribution, α. This parameter is known for dictating the appearance of extended states in the middle of the band [49,54], thus allowing for sending single-particle pulses outwards while still maintaining part of the wave-function amplitude at the center of the chain. We also studied the propagation of entanglement from an initial maximally entangled Bell state through the chain and found that there is a significant improvement in the transmission coefficient by increasing α.

In general, correlated disorder may naturally be present in solid-state devices due to the lack of full experimental control over the system itself as well as over the surroundings. However, as long as internal correlations of a specific kind generate the desired eigenfunctions profile, it should be much more convenient to cope with disorder than fighting against it, since the latter strategy may demand more resources. In other words, when designing a given quantum information processing protocol to be realized in a disordered system, one could think of increasing the amount of correlations of such a disorder, instead of trying to get rid of it.

Although we have considered only diagonal disorder, a similar behavior is expected for off-diagonal fluctuations, i.e., a disordered set of exchange interactions albeit with some quantitative differences [54]. In principle, our findings can be probed in, e.g., ultracold atoms in optical lattices [25] in which great advances such as single-site addressing [24] have been achieved.

Further extensions of our work include investigating the role of internal correlations in disordered channels for high-fidelity state transfer based on weakly coupled communicating parties [4,27,43]. In these models, even though the bulk of the chain is usually weakly populated during the transmission process, the presence of extended eigenstates in the bulk is crucial to support long-distance communication protocols.

ACKNOWLEDGMENTS

This work was partially supported by CNPq (Conselho Nacional de Desenvolvimento Científico e Tecnológico), Grant No. 152722/2016-5, CAPES (Coordenao de Aperfeiçoamento de Pessoal de Ensino Superior, FINEP (Financiadora de Estudos e Projetos), and FAPEAL (Fundação de Amparo à Pesquisa do Estado de Alagoas). T.J.G.A. acknowledges support from the Collaborative Project QuProCS (Grant No. 641277).

[1] S. Bose, Phys. Rev. Lett. **91**, 207901 (2003).
[2] M. Christandl, N. Datta, A. Ekert, and A. J. Landahl, Phys. Rev. Lett. **92**, 187902 (2004).
[3] M. B. Plenio, J. Hartley, and J. Eisert, New J. Phys. **6**, 36 (2004).
[4] A. Wójcik, T. Łuczak, P. Kurzyński, A. Grudka, T. Gdala, and M. Bednarska, Phys. Rev. A **72**, 034303 (2005).
[5] Y. Li, T. Shi, B. Chen, Z. Song, and C.-P. Sun, Phys. Rev. A **71**, 022301 (2005).

[6] M. X. Huo, Y. Li, Z. Song, and C. P. Sun, Europhys. Lett. **84**, 30004 (2008).

[7] G. Gualdi, V. Kostak, I. Marzoli, and P. Tombesi, Phys. Rev. A **78**, 022325 (2008).

[8] L. Banchi, T. J. G. Apollaro, A. Cuccoli, R. Vaia, and P. Verrucchi, Phys. Rev. A **82**, 052321 (2010); New J. Phys. **13**, 123006 (2011).

[9] T. J. G. Apollaro, L. Banchi, A. Cuccoli, R. Vaia, and P. Verrucchi, Phys. Rev. A **85**, 052319 (2012).

[10] S. Lorenzo, T. J. G. Apollaro, A. Sindona, and F. Plastina, Phys. Rev. A **87**, 042313 (2013).

[11] S. Lorenzo, T. J. G. Apollaro, S. Paganelli, G. M. Palma, and F. Plastina, Phys. Rev. A **91**, 042321 (2015).

[12] L. Amico, A. Osterloh, F. Plastina, R. Fazio, and G. M. Palma, Phys. Rev. A **69**, 022304 (2004).

[13] T. J. G. Apollaro and F. Plastina, Phys. Rev. A **74**, 062316 (2006).

[14] F. Plastina and T. J. G. Apollaro, Phys. Rev. Lett. **99**, 177210 (2007); T. J. Apollaro, A. Cuccoli, A. Fubini, F. Plastina, and P. Verrucchi, Phys. Rev. A **77**, 062314 (2008).

[15] M. J. Hartmann, M. E. Reuter, and M. B. Plenio, New J. Phys. **8**, 94 (2006).

[16] D. I. Tsomokos, M. J. Hartmann, S. F. Huelga, and M. B. Plenio, New J. Phys. **9**, 79 (2007).

[17] L. Campos Venuti, S. M. Giampaolo, F. Illuminati, and P. Zanardi, Phys. Rev. A **76**, 052328 (2007).

[18] T. S. Cubitt and J. I. Cirac, Phys. Rev. Lett. **100**, 180406 (2008).

[19] S. M. Giampaolo and F. Illuminati, Phys. Rev. A **80**, 050301 (2009); New J. Phys. **12**, 025019 (2010).

[20] G. Gualdi, S. M. Giampaolo, and F. Illuminati, Phys. Rev. Lett. **106**, 050501 (2011).

[21] M. P. Estarellas, I. D'Amico, and T. P. Spiller, Phys. Rev. A **95**, 042335 (2017); Sci. Rep. **7**, 42904 (2017).

[22] J. I. Cirac, P. Zoller, H. J. Kimble, and H. Mabuchi, Phys. Rev. Lett. **78**, 3221 (1997).

[23] P. Cappellaro, C. Ramanathan, and D. G. Cory, Phys. Rev. A **76**, 032317 (2007); G. A. Álvarez and D. Suter, Phys. Rev. Lett. **104**, 230403 (2010).

[24] C. Weitenberg, M. Endres, J. F. Sherson, M. Cheneau, P. Schausz, T. Fukuhara, I. Bloch, and S. Kuhr, Nature (London) **471**, 319 (2011).

[25] T. Fukuhara, A. Kantian, M. Endres, M. Cheneau, P. Schausz, S. Hild, D. Bellem, U. Schollwock, T. Giamarchi, C. Gross, I. Bloch, and S. Kuhr, Nat. Phys. **9**, 235 (2013); T. Fukuhara, S. Hild, J. Zeiher, P. Schauß, I. Bloch, M. Endres, and C. Gross, Phys. Rev. Lett. **115**, 035302 (2015).

[26] D. G. Angelakis, M. F. Santos, and S. Bose, Phys. Rev. A **76**, 031805(R) (2007).

[27] G. M. A. Almeida, F. Ciccarello, T. J. G. Apollaro, and A. M. C. Souza, Phys. Rev. A **93**, 032310 (2016).

[28] A. Romito, R. Fazio, and C. Bruder, Phys. Rev. B **71**, 100501 (2005); M. W. Johnson, M. H. S. Amin, S. Gildert, T. Lanting, F. Hamze, N. Dickson, R. Harris, A. J. Berkley, J. Johansson, P. Bunyk, E. M. Chapple, C. Enderud, J. P. Hilton, K. Karimi, E. Ladizinsky, N. Ladizinsky, T. Oh, I. Perminov, C. Rich, M. C. Thom, E. Tolkacheva, C. J. S. Truncik, S. Uchaikin, J. Wang, B. Wilson, and G. Rose, Nature (London) **473**, 194 (2011).

[29] Y. Ping, B. W. Lovett, S. C. Benjamin, and E. M. Gauger, Phys. Rev. Lett. **110**, 100503 (2013).

[30] M. Bellec, G. M. Nikolopoulos, and S. Tzortzakis, Opt. Lett. **37**, 4504 (2012).

[31] G. M. A. Almeida and A. M. C. Souza, Phys. Rev. A **87**, 033804 (2013).

[32] D. L. Feder, Phys. Rev. Lett. **97**, 180502 (2006).

[33] E. I. Kuznetsova and A. I. Zenchuk, Phys. Lett. A **372**, 6134 (2008).

[34] A. Wójcik, T. Łuczak, P. Kurzyński, A. Grudka, T. Gdala, and M. Bednarska, Phys. Rev. A **75**, 022330 (2007).

[35] P. J. Pemberton-Ross and A. Kay, Phys. Rev. Lett. **106**, 020503 (2011).

[36] S. Paganelli, S. Lorenzo, T. J. G. Apollaro, F. Plastina, and G. L. Giorgi, Phys. Rev. A **87**, 062309 (2013).

[37] C. K. Burrell and T. J. Osborne, Phys. Rev. Lett. **99**, 167201 (2007); J. Allcock and N. Linden, *ibid.* **102**, 110501 (2009).

[38] S. Lorenzo, F. Lombardo, F. Ciccarello, and G. M. Palma, Sci. Rep. **7**, 42729 (2017).

[39] G. De Chiara, D. Rossini, S. Montangero, and R. Fazio, Phys. Rev. A **72**, 012323 (2005).

[40] J. Fitzsimons and J. Twamley, Phys. Rev. A **72**, 050301 (2005).

[41] D. Burgarth and S. Bose, New J. Phys. **7**, 135 (2005).

[42] D. Petrosyan, G. M. Nikolopoulos, and P. Lambropoulos, Phys. Rev. A **81**, 042307 (2010).

[43] N. Y. Yao, L. Jiang, A. V. Gorshkov, Z.-X. Gong, A. Zhai, L.-M. Duan, and M. D. Lukin, Phys. Rev. Lett. **106**, 040505 (2011).

[44] A. Zwick, G. A. Álvarez, J. Stolze, and O. Osenda, Phys. Rev. A **84**, 022311 (2011); **85**, 012318 (2012).

[45] M. Bruderer, K. Franke, S. Ragg, W. Belzig, and D. Obreschkow, Phys. Rev. A **85**, 022312 (2012).

[46] A. Kay, Phys. Rev. A **93**, 042320 (2016).

[47] P. W. Anderson, Phys. Rev. **109**, 1492 (1958); E. Abrahams, P. W. Anderson, D. C. Licciardello, and T. V. Ramakrishnan, Phys. Rev. Lett. **42**, 673 (1979).

[48] D. H. Dunlap, H.-L. Wu, and P. W. Phillips, Phys. Rev. Lett. **65**, 88 (1990); P. Phillips and H.-L. Wu, Science **252**, 1805 (1991).

[49] F. A. B. F. de Moura and M. L. Lyra, Phys. Rev. Lett. **81**, 3735 (1998).

[50] F. M. Izrailev and A. A. Krokhin, Phys. Rev. Lett. **82**, 4062 (1999).

[51] U. Kuhl, F. M. Izrailev, A. A. Krokhin, and H.-J. Stöckmann, Appl. Phys. Lett. **77**, 633 (2000).

[52] U. Kuhl, F. M. Izrailev, and A. A. Krokhin, Phys. Rev. Lett. **100**, 126402 (2008); O. Dietz, U. Kuhl, H.-J. Stöckmann, N. M. Makarov, and F. M. Izrailev, Phys. Rev. B **83**, 134203 (2011).

[53] F. Izrailev, A. Krokhin, and N. Makarov, Phys. Rep. **512**, 125 (2012).

[54] R. P. A. Lima, M. L. Lyra, E. M. Nascimento, and A. D. de Jesus, Phys. Rev. B **65**, 104416 (2002); F. A. B. F. de Moura, M. D. Coutinho-Filho, E. P. Raposo, and M. L. Lyra, *ibid.* **66**, 014418 (2002); D. Nunes, A. R. Neto, and F. de Moura, J. Magn. Magn. Mater. **410**, 165 (2016).

[55] F. A. B. F. de Moura, M. D. Coutinho-Filho, E. P. Raposo, and M. L. Lyra, Phys. Rev. B **68**, 012202 (2003).

[56] F. Domínguez-Adame, V. A. Malyshev, F. A. B. F. de Moura, and M. L. Lyra, Phys. Rev. Lett. **91**, 197402 (2003).

[57] J. Rodriguez-Laguna, S. N. Santalla, G. Ramírez, and G. Sierra, New J. Phys. **18**, 073025 (2016).

[58] C.-K. Peng, S. V. Buldyrev, A. L. Goldberger, S. Havlin, F. Sciortino, M. Simons, and H. E. Stanley, Nature (London) **356**, 168 (1992); P. Carpena, P. Bernaola-Galvan, P. C. Ivanov, and H. E. Stanley, *ibid.* **418**, 955 (2002).
[59] B. A. Carreras, B. van Milligen, M. A. Pedrosa, R. Balbín, C. Hidalgo, D. E. Newman, E. Sánchez, M. Frances, I. García-Cortés, J. Bleuel, M. Endler, S. Davies, and G. F. Matthews, Phys. Rev. Lett. **80**, 4438 (1998).
[60] C.-H. Lam and L. M. Sander, Phys. Rev. Lett. **69**, 3338 (1992).
[61] M. Paczuski, S. Maslov, and P. Bak, Phys. Rev. E **53**, 414 (1996).
[62] J. Feder, *Fractals* (Plenum Press, New York, 1988).
[63] W. K. Wootters, Phys. Rev. Lett. **80**, 2245 (1998).
[64] D. ben Avraham, E. Bollt, and C. Tamon, Quantum Inf. Process. **3**, 295 (2004).
[65] N. Konno, Phys. Rev. E **72**, 026113 (2005).
[66] M. Horodecki, P. Horodecki, and R. Horodecki, Phys. Rev. Lett. **80**, 5239 (1998).
[67] D. J. Thouless, Phys. Rep. **13**, 93 (1974).
[68] V. Coffman, J. Kundu, and W. K. Wootters, Phys. Rev. A **61**, 052306 (2000).